Russian Journal of Earth Sciences Online ISSN: 1681-1208

Special Issue: "Kamchatka Earthquake M 8.8 on July 29, 2025"

Anomalous Changes in Ionospheric Parameters During the Preparation and Occurrence of the $M8.8$ Earthquake and a Series of Earthquakes With $M \geq 6$ That Occurred Near the Kamchatka Peninsula From June to September 2025 According to the Data of Satellite Navigation Systems

V. G. Bondur*[,1], M. N. Tsidilina[1], O. S. Voronova[1], M. V. Gaponova[1], and G. A. Timoshina[1]

[1] Institute for Scientific Research of Aerospace Monitoring "AEROCOSMOS", Moscow, Russian Federation
* **Correspondence to:** Valery Bondur, office@aerocosmos.info

Abstract: Changes in the altitude profiles of the ionospheric electron density (N_e) and the total electron content (TEC) were detected using satellite navigation system data during the preparation and occurrence of a powerful $M8.8$ earthquake (July 29, 2025, UTC) and other strong earthquakes of $M \geq 6$ that occurred near the Kamchatka Peninsula in June–September 2025. A 9–18% decrease in the ionospheric electron density was detected, occurred 1–5 days before the $M8.8$ earthquake. A gradual decrease in the total electron content (TEC) began 3 months before the earthquake, ceasing 15 days before the event. Using the Long Short-Term Memory and Autoencoder neural networks, anomalies were identified in the time series of normalized values of the total electron content (NTEC) of the ionosphere during the preparation of earthquakes of $M \geq 6$ that occurred in June–September 2025 near the Kamchatka Peninsula. The pattern of the anomalous variations in ionospheric parameters identified in this research corresponds to the characteristics of ionospheric anomalies during the preparation and occurrence of strong seismic events presented in earlier works.

Keywords: Remote sensing, ionospheric electron density, total electron content, seismo-ionospheric coupling, ionospheric anomalies, Kamchatka megathrust earthquake

Citation: Bondur V. G., Tsidilina M. N., Voronova O. S., Gaponova M. V., and Timoshina G. A. (2026), Anomalous Changes in Ionospheric Parameters During the Preparation and Occurrence of the $M8.8$ Earthquake and a Series of Earthquakes With $M \geq 6$ That Occurred Near the Kamchatka Peninsula From June to September 2025 According to the Data of Satellite Navigation Systems, *Russian Journal of Earth Sciences*, 26, ES2017, EDN: ZFBUIU, https://doi.org/10.2205/2026es001127

1. Introduction

On July 29, 2025 (UTC), a tsunamigenic $M8.8$ earthquake occurred off the coast of the Kamchatka Peninsula, marking the strongest seismic event in the last 73 years. This earthquake was accompanied by significant foreshocks and aftershocks with $M \geq 6$ (http://www.ceme.gsras.ru, https://www.emsd.ru, http://earthquake.usgs.gov, https://www.emsc-csem.org). Due to the seismic resilience of buildings and the timely evacuation of the population from tsunami-affected areas on the Kamchatka Peninsula and the Kuril Islands, casualties and severe destruction were avoided. Minor injuries were reported among four individuals, along with cracks in buildings, coastal infrastructure was also damaged by tsunami waves.

In contrast, during an $M7.1$ earthquake that struck in this region in the small town of Neftegorsk (Sakhalin Island) on May 28, 1995, nearly the entire population of the settlement (over 2000 people) died, and the small town was completely destroyed [*Oskorbin et al.*, 2001].

Research Article

Received: February 2, 2026
Accepted: May 25, 2026
Published: July 1, 2026

Another effect of the strong earthquakes occurred in the Kuril-Kamchatka region in 2025 was the activation of volcanic activity. As a result of the intense seismic events that took place in this seismically hazardous area from July to September 2025, the Krasheninnikova volcano, which last erupted 400 years ago, became active. The activity of the Klyuchevskoy, Karymsky, Shiveluch, and Ebeko volcanoes also increased (https://www.emsd.ru).

In light of this, any proactive measures aimed at mitigating the effects of strong earthquakes are highly relevant: constructing earthquake-resistant buildings and structures [*Fedotov*, 2005], ensuring preparedness of emergency services and authorities for rapid response [*Natural Hazards...*, 2000]. To achieve this, it is necessary to obtain real-time information about seismic hazards and to predict the location, timing, and magnitude of future earthquakes. Therefore, conducting scientific research to identify medium- and short-term precursors of earthquakes is an extremely important yet challenging task [*Chebrov et al.*, 2013; *Mogi*, 1985; *Sobolev and Ponomarev*, 2003].

Such precursors include ionospheric anomalies associated with earthquakes, which manifest as specific variations in parameters of space plasma [*Bondur and Smirnov*, 2005; *Bondur et al.*, 2024, 2022, 2021; *Pulinets et al.*, 2010; *Zolotov et al.*, 2013], electric and magnetic fields, as well as characteristics of electromagnetic waves [*Gokhberg and Shalimov*, 2000; *Liperovsky et al.*, 1992; *Pulinets and Boyarchuk*, 2004]. The possible pathways through which seismic disturbances affect the ionosphere are typically considered to be electromagnetic [*Freund*, 2011; *Liperovsky et al.*, 2008; *Namgaladze and Karpov*, 2015; *Pulinets et al.*, 2010, 2015; *Sorokin and Ruzhin*, 2015] and atmospheric-wave channels, including acoustic-gravity and internal gravity waves [*Gokhberg and Shalimov*, 2000; *Liperovsky et al.*, 2008; *Sorokin and Hayakawa*, 2013].

One area of contemporary research of variations in ionospheric parameters involves analyzing data obtained from satellites such as Ionosphere-M, Swarm, and others (https://www.roscosmos.ru) and [*Akhoondzadeh et al.*, 2018; *Parrot et al.*, 2016], as well as data from Global Navigation Satellite Systems (GNSS) like GLONASS, GPS, etc [*Bondur and Smirnov*, 2005; *Pulinets et al.*, 2015; *Zhu and Jiang*, 2020], and ground-based vertical sounding data [*Bychkov et al.*, 2017].

Currently, one of the effective means of monitoring ionospheric parameters aimed at detection of specific variations related to impending earthquakes is through the use of GNSS (GPS, GLONASS, etc.), which allow for continuous data collection from virtually any point on Earth.

A large dataset from global navigation satellite systems and the synthesis of data-based research findings on the features of ionospheric parameter variations prior to earthquakes revealed a statistical correlation between significant seismic events and anomalous disturbances in the ionosphere [*Bondur and Smirnov*, 2005; *Bondur et al.*, 2024, 2022, 2021; *Pulinets et al.*, 2010; *Pulinets and Boyarchuk*, 2004].

This paper presents the research results of anomalies in ionospheric parameters recorded using satellite navigation systems during the preparation and occurrence of a powerful $M8.8$ earthquake that occurred on July 29, 2025 (UTC), in the Kamchatka Peninsula region, as well as its foreshocks and aftershocks with $M \geq 6$.

2. Methods of Research and Data Used

The study of changes in the ionosphere occurring from January 1 to September 30, 2025, during the preparation and occurrence of strong earthquakes with $M \geq 6$ in the Kamchatka Peninsula region, was conducted using data from global navigation satellite systems (GLONASS, GPS, Galileo, Beidou, QZSS, IRNSS, SBAS), obtained from the archives of the Geophysical Survey of the Russian Academy of Sciences (http://gps.gsras.ru, 2025) and NASA (https://www.earthdata.nasa.gov/, 2001–2025), within the studied area near the Kamchatka Peninsula.

When selecting the size of the studied area, it was taken into account that the radius of an earthquake preparation zone is [*Dobrovolsky et al.*, 1979]:

$$R = 10^{0.43M}$$

where M is the magnitude of the earthquake.

For $M6.0$ earthquakes, the size of a seismic activation area is approximately 400 km, while for the $M8.8$ earthquake, a zone with a significantly larger radius (up to several thousand kilometers) should be analyzed. Considering this, the studied area was selected, as shown in Figure 1b.

At the beginning of the research, a joint analysis was conducted on the seismic regime of the region and the heliogeophysical situation. To exclude the contribution to ionospheric disturbances from geomagnetic field variations occurred during the research period, an analysis of changes in the geomagnetic index Dst was carried out using data from the World Data Center for Geomagnetism, Kyoto (http://wdc.kugi.kyoto-u.ac.jp/index.html, 2025). Additionally, changes in the solar activity index F10.7 were also analyzed based on the data from the National Research Council Canada and Natural Resources Canada (https://www.spaceweather.gc.ca/index-en.php, 2025).

During the research on seismo-ionospheric coupling, changes in the altitude profiles of the ionospheric electron density (N_e) and ionospheric total electron content (TEC) were analyzed.

The study of variations in profiles of the ionospheric electron density was conducted using the methodology described in [*Bondur and Smirnov*, 2005]. This methodology is based on retrieval of ionospheric parameters by implementing the method of radio probing, which utilizes measurements of radio signal parameters recorded by ground stations of satellite navigation systems located in the studied regions. In this case, an algorithm is implemented for solving inverse problems of refraction of radio waves, which are inherently unstable and require special mathematical methods to account for additional information regarding the task [*Bondur and Smirnov*, 2005]. The methodology allowed for recording height distributions of ionospheric electron density from a single ground station, which is particularly important for remote and hard-to-access regions of the Earth.

As a result of navigation data processing for the period from July 12 to August 5, 2025, N_e height profiles for altitudes from 80 to 1000 km were obtained along trajectories of sub-ionospheric points with a discretization of 30 seconds. These profiles were constructed using data from GPS satellites No. 1, No. 21 and No. 15, recorded at PETS site (53.01°N, 158.39°E) and MAG0 site (59.34°N, 150.46°E) (Figure 3).

Changes in ionospheric total electron content (TEC) were also analyzed using GNSS data presented in IONEX format. These data contain TEC values with a resolution of 2.5° in latitude (from 87.5°N to 87.5°S) and 5.0° in longitude (from 180°E to 180°W) with a two-hour interval (https://www.earthdata.nasa.gov/) and [*Noll*, 2010]. The modeling and extrapolation procedures used to construct TEC distributions allowed for obtaining data for the studied territory with a limited number of ground stations [*Noll*, 2010]. Despite the low spatial resolution of these maps, they provide the best accessibility and greatest operational use of the data.

To identify seismo-ionospheric variations from January 1 to September 30, 2025, TEC values were analyzed using several approaches:

1. Conducting a comparison of the time series of TEC values from January 1 to September 30, 2025 with long-term average TEC values within the analyzed area (47.5–55.0°N, 155–165°E) for each two-hour interval.
2. Analyzing relative values of total electron content in the ionosphere DTEC:

$$\mathrm{DTEC} = \frac{\mathrm{TEC} - \mathrm{MTEC}}{\mathrm{MTEC}} \times 100\%$$

where TEC represents the total electron content values for the current day in 2025; MTEC represents the median values calculated using a sliding window of 10 days with a step of 1 day.

Based on the obtained data, global and local DTEC maps were constructed and analyzed. For the studied area (47.5–55.0°N, 155–165°E), two-dimensional distributions of DTEC were also constructed and analyzed, along with graphs showing changes in DTEC for each two-hour interval.

3. Normalized values of total electron content (NTEC) were calculated based on multi-year data:

$$NTEC = (TEC - \mu)/\sigma$$

where TEC represents the total electron content values for the current day in 2025; μ is the arithmetic mean of TEC from 2001 to 2024, and σ is the standard deviation for the studied day from 2001 to 2024.

4. Analysis of the generated time series of NTEC values using neural networks for the area with coordinates: 47.5–55.0°N, 155–165°E. The identification of anomalies in the NTEC time series was carried out using two types of neural networks: Long Short-Term Memory (LSTM) [*Bhandarkar et al.*, 2019] and Autoencoder (AE) [*Xue et al.*, 2022].

The architecture of the LSTM neural network included a layer with 50 neurons as well as a Dropout layer to prevent overfitting. Additionally, a fully connected output layer was added. The LSTM neural network utilized a mean squared error loss function, which is sensitive to large deviations, necessary for detecting anomalies in the NTEC time series [*Yurtin*, 2024]. The use of the LSTM neural network enabled analysis of time series by training on sequences of data with cross-validation to enhance result reliability.

Next, to identify anomalies in these formed time series of trained data, an Autoencoder (AE) neural network was used, consisting of an input layer, encoding layer, and decoding layer. The encoding layer allowed compressing the input data into a more compact form, while the decoding layer then reconstructed the original data from this compressed form. Thresholds calculated as the mean value of the NTEC time series plus two standard deviations ($\mu+2\sigma$) and plus three standard deviations ($\mu+3\sigma$) were used to detect anomalies.

Below are the results of the studies conducted using the described methodology.

3. Research Results and Their Analysis

3.1. Seismic Regime of the Studied Region and Heliogeophysical Conditions

The analysis of the seismic regime of the Kuril-Kamchatka arc was conducted for the period from January 1 to September 30, 2025. The following earthquake times/dates are given in local time.

Figure 1a shows the distribution of earthquakes with $M \geq 4.0$ during this period. From Figure 1a, it can be seen that the studied period can be divided into two parts: from January 1 to July 19, 2025, and from July 20 to September 30, 2025. From January 1 to July 19, 2025, the seismic activity was characterized as low. Earthquakes with $M = 4.0$–4.9 predominated (123 earthquakes). There were also 11 earthquakes with $5.0 \leq M \leq 5.8$ and one $M6.0$ earthquake (June 14, 2025, LT) (http://www.ceme.gsras.ru, http://earthquake.usgs.gov).

The period from July 20 to September 30, 2025 was characterized by high seismic activity (Figure 1a).

Figure 1b presents a schematic representation of the epicenters of earthquakes with $M = 4.0$–8.8 during this period on the studied area near the Kamchatka Peninsula.

A total of 2650 earthquakes occurred in the studied area from July 20 to September 30, 2025, including:

- one $M8.8$ earthquake (July 30, 2025, LT (July 29, 2025, UTC);
- two earthquakes with $M = 7.4$ (July 20 and September 13, 2025, LT);
- one $M7.8$ earthquake (July 19, 2025, LT);

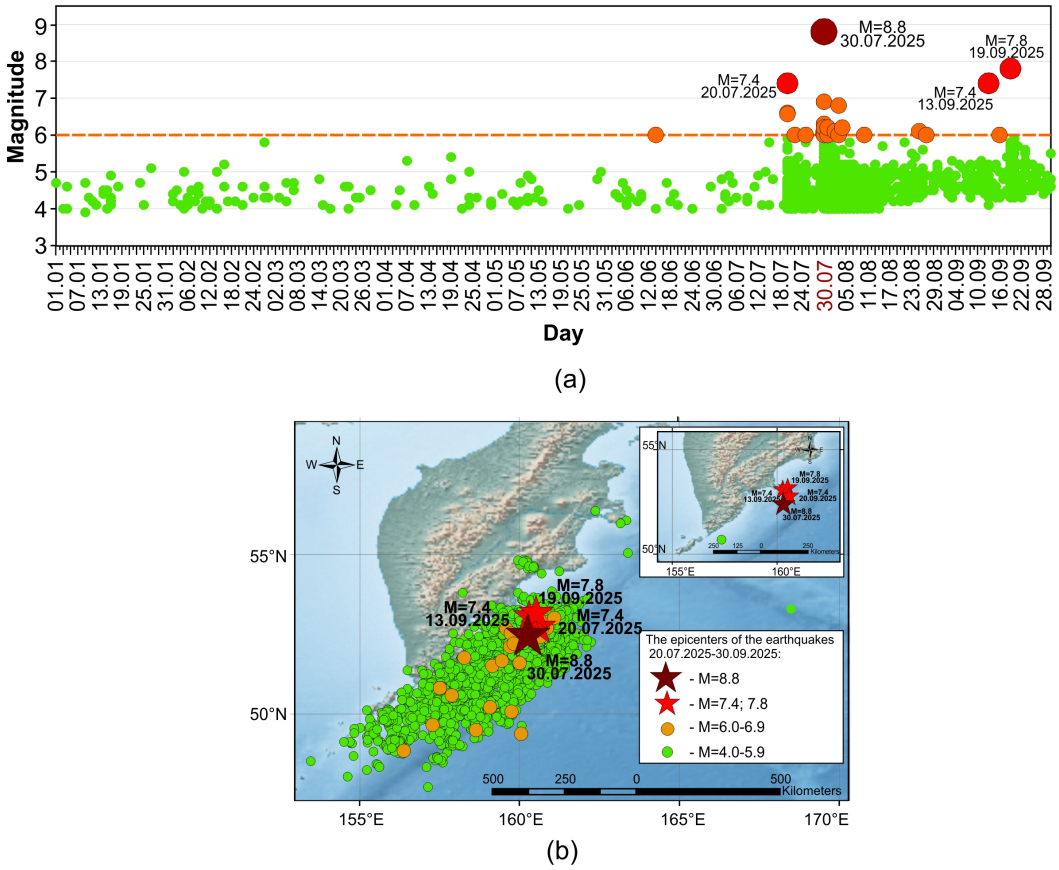

Figure 1. Distribution of earthquakes with $M \geq 4.0$ from January 1 to September 30, 2025 (a) and a schematic representation of the epicenters of earthquakes in the studied area of the Kuril-Kamchatka arc (b) during the period from July 20 to September 30, 2025.

- 22 earthquakes with $6.0 \leq M \leq 6.9$;
- 391 earthquakes with $5.0 \leq M \leq 5.9$;
- 2233 earthquakes with $4.0 \leq M \leq 4.9$.

Table 1 provides information about earthquakes with $M \geq 6$ that occurred between July 20 and September 30, 2025. The strongest $M8.8$ shock was recorded on July 30, 2025, at 11:24 local time (July 29, 2025, at 23:24 UTC) at coordinates 52.498°N, 160.264°E (information about this earthquake is highlighted in red in Table 1) (http://www.ceme.gsras.ru, https://www.emsd.ru, http://earthquake.usgs.gov, https://www.emsc-csem.org).

The $M8.8$ earthquake on July 30, 2025 (July 29, 2025, UTC), became the strongest tsunamigenic earthquake in the Kamchatka seismic zone since 1952. The epicenter of this earthquake was located less than 30 km from the epicenter of the tsunamigenic $M9.0$ earthquake, that occurred on November 4, 1952.

Before a powerful $M8.8$ earthquake, foreshocks were recorded: on June 14, 2025, ($M6.0$ earthquake), on July 20, 2025, (three earthquakes with $M = 6.6$ and one earthquake with $M = 7.4$), and on July 22 and July 25, 2025, two earthquakes with $M = 6.0$ occurred (Figure 1 and Table 1).

After the main $M8.8$ shock on July 30, 2025, seven aftershocks with $M = 6.0$–6.9 were recorded (http://www.ceme.gsras.ru, https://www.emsd.ru, http://earthquake.usgs.gov, https://www.emsc-csem.org). On that day, a large number of smaller magnitude earthquakes were also registered.

Aftershocks with $M \geq 6.0$ were recorded on July 31; August 2, 3, 4, 10, 25, 27; and on September 13, 16, and 19, 2025, including two earthquakes with $M = 7.4$ (September 13, 2025) and $M = 7.8$ (September 19, 2025) (Figure 1 and Table 1) (http://www.ceme.gsras.ru, https://www.emsd.ru, http://earthquake.usgs.gov, https://www.emsc-csem.org).

Table 1. Information about earthquakes with $M \geq 6$ occurred in the studied area of the Kamchatka Peninsula (47.5–55.0°N, 155–165°E) from July 20 to September 30, 2025

No.	Date (LT)	Time (LT)	Latitude	Longitude	Depth (km)	Magnitude
1	20.07.2025	18:28:17.860	52.928	160.623	23.0	6.6
2	20.07.2025	19:07:42.573	52.698	160.833	10.0	6.6
3	20.07.2025	19:23:00.264	52.870	160.793	22.1	6.6
4	20.07.2025	18:49:04.327	52.830	160.682	34.0	7.4
5	22.07.2025	13:59:28.404	52.413	160.645	12.3	6.0
6	25.07.2025	10:37:27.147	53.015	161.062	14.0	6.0
7	30.07.2025 (29.07.2025, UTC)	11:24:52.480	52.498	160.264	35.0	8.8
8	30.07.2025	11:30:03.032	52.520	159.703	16.4	6.3
9	30.07.2025	11:30:44.566	52.650	159.578	25.4	6.1
10	30.07.2025	11:36:01.341	51.754	158.250	35.0	6.0
11	30.07.2025	11:37:34.403	51.509	159.126	35.0	6.0
12	30.07.2025	21:56:13.780	51.604	160.001	10.4	6.1
13	30.07.2025	12:16:06.520	52.105	159.692	35.0	6.2
14	30.07.2025	12:09:58.961	52.195	159.800	36.6	6.9
15	31.07.2025	04:07:46.668	49.670	157.274	35.0	6.0
16	31.07.2025	17:27:14.259	49.500	158.627	12.0	6.2
17	02.08.2025	06:20:45.191	50.209	159.065	10.0	6.1
18	03.08.2025	02:14:07.279	51.675	159.426	45.6	6.0
19	03.08.2025	17:37:55.148	50.585	157.864	30.0	6.8
20	04.08.2025	16:20:54.562	48.859	156.366	16.0	6.2
21	10.08.2025	02:04:07.171	50.072	159.736	11.0	6.0
22	25.08.2025	18:48:34.882	49.392	160.036	10.0	6.1
23	27.08.2025	15:49:51.922	50.824	157.496	53.4	6.0
24	13.09.2025	14:37:54.754	53.104	160.294	39.4	7.4
25	16.09.2025	04:34:36.629	52.692	160.703	24.4	6.0
26	19.09.2025	06:58:13.903	53.193	160.513	19.5	7.8

To exclude the contribution of geomagnetic field variations that occurred from January 1 to September 30, 2025, to ionospheric disturbances, an analysis of changes in the geomagnetic index (http://wdc.kugi.kyoto-u.ac.jp/index.html, 2025). The results are shown in Figure 2a.

From the analysis of Figure 2a, it follows that from January 1 to June 15, 2025, the geomagnetic field of the Earth was quite disturbed. Numerous geomagnetic disturbances ranging from moderate to strong were recorded. Strong geomagnetic disturbances were registered on January 2, 2025 (Dst = –221 nT), April 17, 2025 (Dst = –138 nT), June 1–3, 2025 (Dst = –101 to –119 nT), and June 14, 2025 (Dst = –101 nT) (Figure 2a).

From June 16 to August 8, 2025, the geomagnetic field of the Earth was calm or weakly disturbed, while from August 9 to September 30, 2025, four moderate geomagnetic storms were recorded (Figure 2a).

Thus, from June 16 to August 8, 2025, the influence of the geomagnetic field on the Earth's ionosphere can be considered insignificant.

In addition, for the period from January 1 to September 30, 2025, a time series of changes in the solar activity index F10.7 was generated using data from the National Research Council Canada and Natural Resources Canada (https://www.spaceweather.gc.ca/index-en.php, 2025) (Figure 2b).

From the analysis of Figure 2b, it follows that the highest values of the F10.7 index were recorded in January and February 2025 (max F10.7 = 222.0 to 239.9 sfu), during the period

from August 27 to August 30, 2025 (F10.7 = 208.4 to 240.1 sfu), and on August 31, 2025 (F10.7 = 316.5 sfu) (Figure 2b).

The registered radio flux at a wavelength of 10.7 cm decreased from April 25 to August 24, 2025 (F10.7 = 113.2 to 168.6 sfu), with maximum values of the solar activity index recorded on June 1, 2025 (F10.7 = 168.6 sfu) and June 16, 2025 (F10.7 = 160.5 sfu).

Thus, during the final stage of preparation and occurrence of a powerful $M8.8$ earthquake (July 30, 2025), solar activity was low.

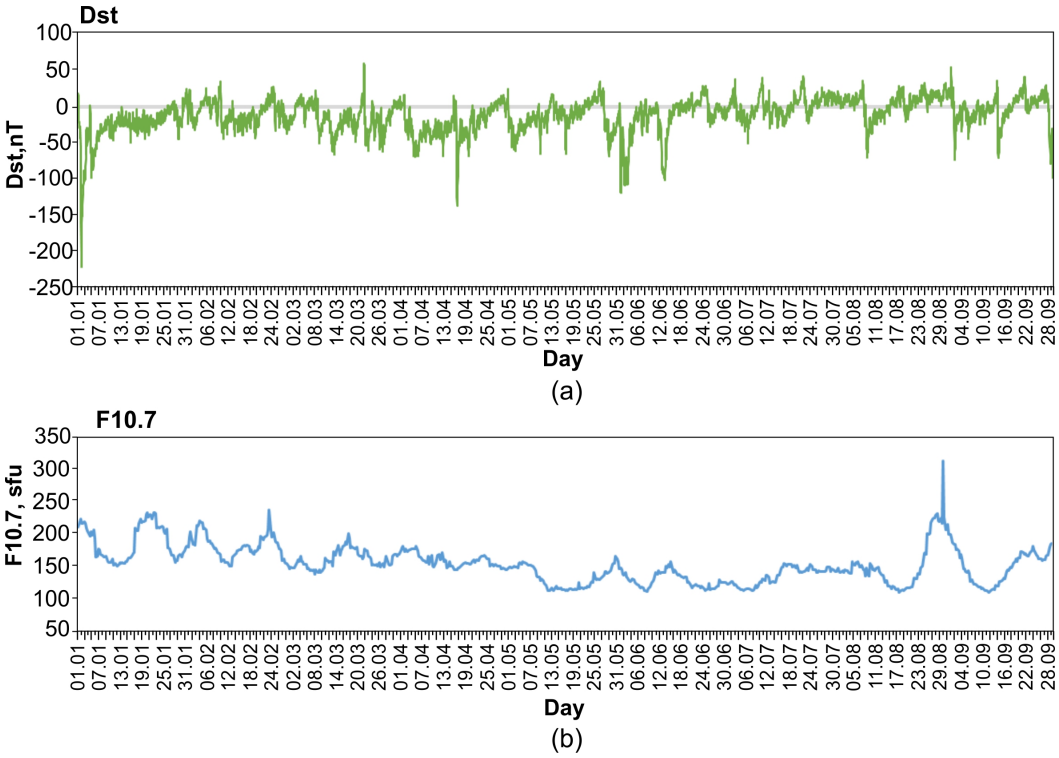

Figure 2. Graphs of changes in the geomagnetic index Dst (a) and the solar activity index F10.7 (b) during the period from January 1 to September 30, 2025.

3.2. Analysis of Changes in Height Profiles of Ionospheric Electron Density

Changes in height profiles of ionospheric electron density (N_e) were analyzed to identify abnormal variations in ionospheric parameters during the preparation and occurrence of the studied earthquakes. Considering the significant size of the zone used for the analysis of anomalous variations in ionospheric parameters, data obtained by PETS and MAG0 sites were selected (Figure 3).

Changes in ionospheric electron density from July 12 to August 5, 2025, were analyzed using data from GPS satellites No. 1, No. 21 (PETS site), and No. 15 (MAG0 site) (Figure 3). These satellites' pass times over the studied territory were: for satellite No. 1 from 6 LT to 11 LT; for satellite No. 21 from 12 LT to 17 LT; for satellite No. 15 from 16 LT to 20 LT.

Figure 4 presents time series of changes in height profiles of ionospheric electron density obtained from data of GPS satellites No. 1 (Figure 4a), No. 21 (Figure 4b), and No. 15 (Figure 4c) during preparation and occurrence of a series of strong earthquakes in the Kamchatka Peninsula area in July–August 2025.

The analysis of data obtained from satellite No. 1, recorded at the PETS site (Figure 4a), during the satellite's pass over the epicentral area in the morning, showed that since July 14, 2025, there was a decrease in N_e values by 8–23% compared to the data recorded on July 13, 2025. Then, on July 15, 2025, the N_e values reached the levels observed on July 13, 2025, and later that same day, a N_e drop of ~ 16% was registered. N_e values remained low until July 16, 2025 (four days before the $M7.4$ earthquake).

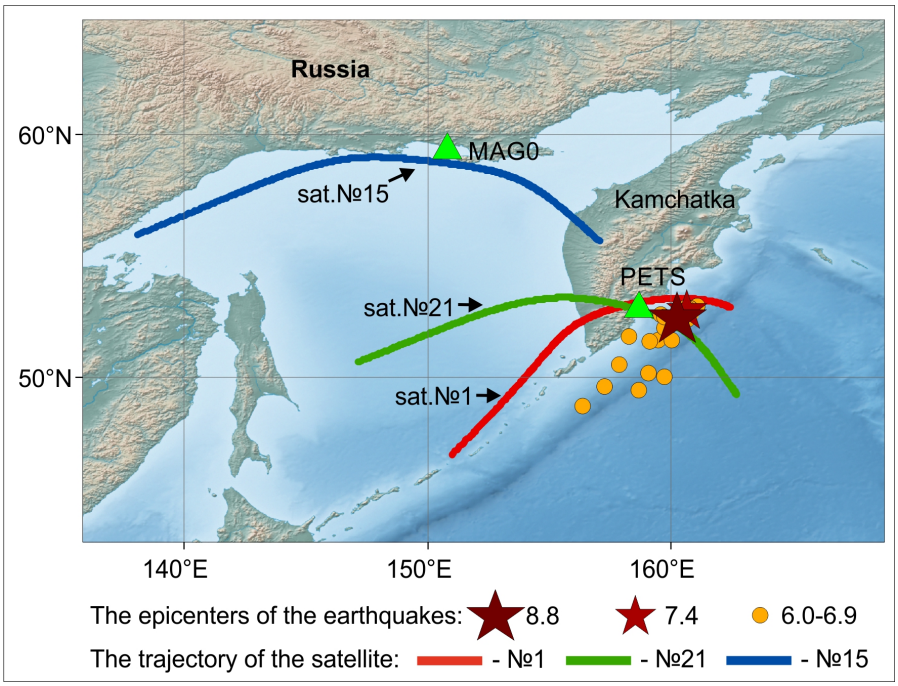

Figure 3. Map of the locations of PETS and MAG0 sites, and the trajectories of the sub-ionospheric points of GPS satellites No. 1, No. 21, and No. 15.

On July 17, 2025 (three days before the earthquake), an increase by ~17% in ionospheric electron density was again recorded (Figure 4a). A slight decrease in N_e was registered on July 20, 2025. On that day, earthquakes with M = 6.6–7.4 occurred. A sharp increase in N_e (by 20%) compared to the previous day was recorded on July 22, 2025 (Figure 4a). On that day, an M6.0 earthquake occurred in the studied area.

From July 23 to July 25, 2025, there was a decrease in N_e (by ~10–19% compared to July 22, 2025), reaching a minimum value on July 25, 2025 (five days before the M8.8 earthquake). However, it should be pointed out that the N_e values from July 23 to July 25, 2025, were higher compared to those recorded from July 12 to July 21, 2025 (Figure 4a).

After July 25, 2025, there was a slight increase in N_e (by ~10–12%) over the next three days. On July 29, 2025, one day before the M8.8 earthquake, a drop in N_e of ~18% was recorded (Figure 4a). Following the main M8.8 seismic event that occurred on July 30, 2025, in Kamchatka, strong aftershocks with M = 6.0–6.9 were recorded throughout that day and the following days. Thus, the ionosphere remained disturbed. Periods of sharp increases, decreases, and again increases in N_e values were registered (Figure 4a).

The analysis of Figure 4b showed that for the data obtained from satellite No. 21 (PETS site) during its daytime pass over the epicentral area, the pattern of change in ionospheric electron density from July 12 to July 22, 2025, was similar to the N_e variations identified from satellite No. 1 data recorded at the same site. Specifically: on July 14, 2025, a decrease in N_e (by ~10%) was recorded; on July 15, 2025, N_e recovered to levels observed on July 13, 2025; on July 16 and July 18, 2025, a drop in N_e of ~ 12–16% compared to the previous day was revealed; and on July 22, 2025, an increase in N_e of ~16–20% was registered (Figure 4b).

In contrast to satellite No. 1 data (Figure 4a), satellite No. 21 data (Figure 4b) showed an increase in electron density that remained on July 23 and 24, 2025, reaching ~17%. Then, on July 25, 2025 (five days before the M8.8 earthquake), a decrease in N_e of ~17% occurred, which remained relatively stable until July 30, 2025. On the day of the earthquake, July 30, 2025, a slight increase in N_e (by ~10%) was detected. From July 31 to August 2, 2025, electron density changed little; however, from August 3, 2025, a decrease in N_e values was observed (Figure 4b).

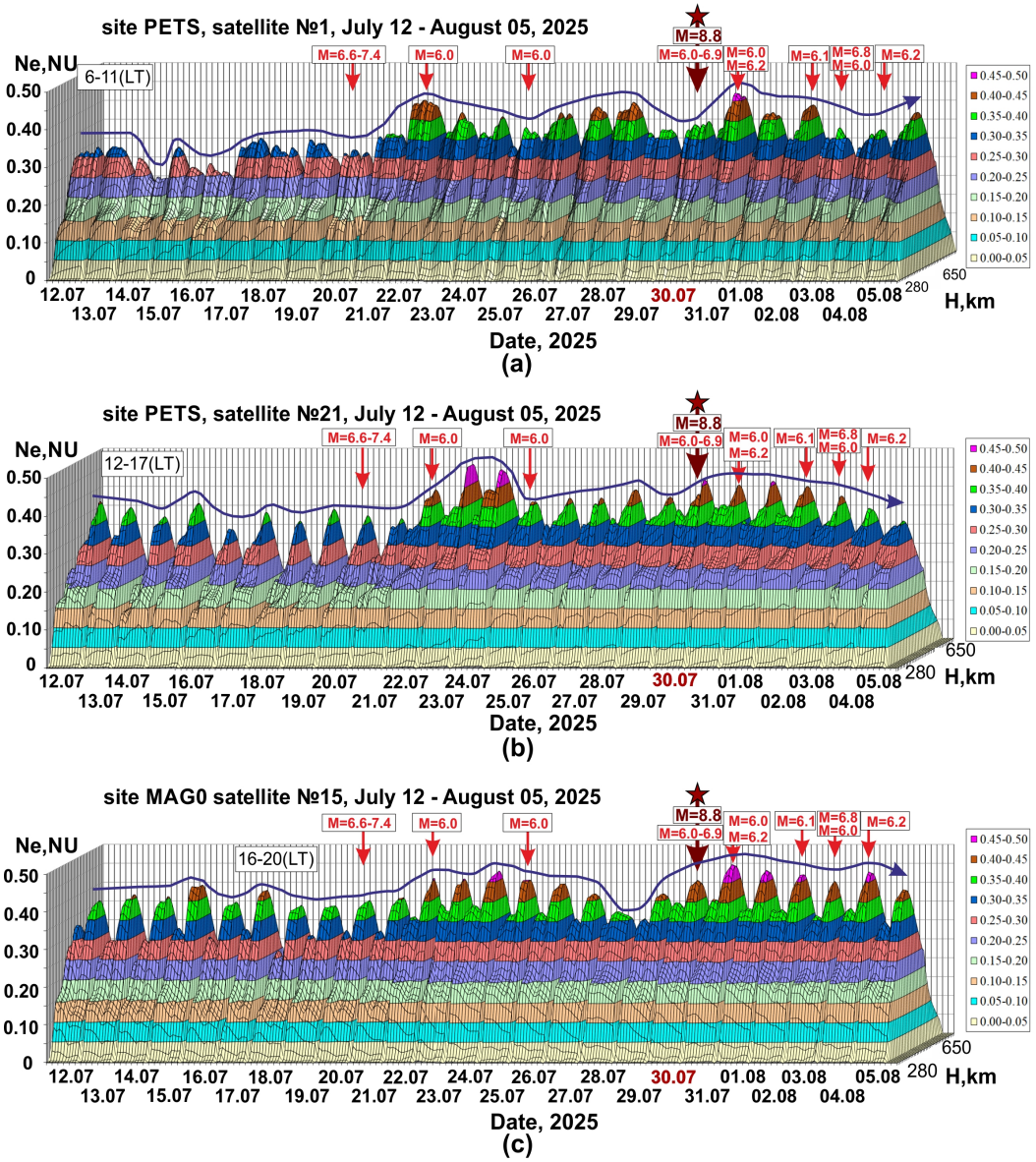

Figure 4. Height profiles of ionospheric electron density from July 12 to August 5, 2025, obtained from data of satellites No. 1 (a), No. 21 (b) at PETS site and No. 15 at MAG0 site.

The analysis of Figure 4c indicated that for data obtained from satellite No. 15 recorded at MAG0 site during its evening pass over the earthquake zone on July 15, 2025, a slight increase in N_e (by ~9%) was detected. The decrease in N_e values recorded the following day on July 16, 2025, amounted to ~ 12% compared to the previous day. Then on July 17, 2025, a slight increase occurred (by ~ 7%). On July 18, 2025 (two days before the $M7.4$ earthquake), a decrease in N_e (by ~ 11%) was observed, and then for the next three days, N_e values changed little (Figure 4c). An increase in N_e of ~ 12% compared to data obtained the previous day was registered on July 22, 2025.

From July 23 to July 26, 2025, values of ionospheric electron density remained high (the maximum N_e value was recorded on July 24, 2025). Then, on July 27, 2025, a decrease in N_e began (by ~ 9%), and on July 28, 2025 (two days before the $M8.8$ earthquake), a decrease in N_e of ~ 12% was recorded. As the date of the $M8.8$ earthquake of approached, N_e began to increase. N_e values remained high until August 4, 2025, and then a decrease in N_e values started (Figure 4c).

Analysis of the height profiles of ionospheric electron density showed that 1, 2, and 5 days before the $M8.8$ earthquake that occurred on July 30, 2025, near the Kamchatka

Peninsula, a decrease in N_e was observed. A decrease in N_e was also registered 2, 4, and 6 days before the $M7.4$ foreshock (July 20, 2025) (Figure 4). The presence of such anomalous features in ionospheric parameters may indicate impending earthquakes.

3.3. Analysis of Changes in Ionospheric Total Electron Content (TEC)

To analyze the changes in ionospheric total electron content (TEC) during the preparation and occurrence of a series of strong earthquakes that occurred in the area of the Kuril-Kamchatka arc in 2025, IONEX data were analyzed for each two-hour interval for the period from 2001 to 2025. Using these data, time series of TEC values were constructed for the period from January 1 to September 30, 2025. In addition, series of average long-term TEC values (μ) and $\mu + 2\sigma$ were formed for the period from 2001 to 2024.

Figure 5 shows, as examples, the time series of values of the TEC characteristics, generated for 2 LT (Figure 5a) and 14 LT (Figure 5b).

From the Figure 5a, it follows that from January 1 to May 2, 2025, according to the data obtained at 2LT, high TEC values were recorded close to the $\mu + 2\sigma$, and on some days, for example, from January 1 to January 7 and from January 22 to January 23, February 25, and from March 20 to March 26, 2025, TEC was higher than $\mu + 2\sigma$. High solar activity (Figure 2b) and geomagnetic disturbances (Figure 2a) were recorded on these days.

From May 3 to July 14, 2025, a trend of overall decrease in TEC values was observed (indicated by the dashed line in Figure 5a), including values below the long-term average recorded on June 4, 2025 (10 days before the $M6.0$ earthquake that occurred on June 14, 2025), as well as on June 15 (the day after this $M6.0$ earthquake) and on July 14, 2025 (6 days before the $M7.4$ earthquake that occurred on July 20, 2025). A trend of increasing TEC values was identified (Figure 5a) from July 15 to July 24, 2025, followed by a decrease in TEC values on July 25–26 and July 28, 2025 (2 and 4–5 days before a powerful $M8.8$ earthquake that occurred on July 30, 2025, LT).

Figure 5a demonstrates that high TEC values close to $\mu + 2\sigma$ remained for four days from July 30 to August 3, 2025 (ten aftershocks with $M = 6.0$–6.9 were recorded during this period), then a decrease in TEC values began on August 3, 2025. A sharp jump in TEC reaching $\mu + 2\sigma$ was detected on August 9, 2025. It was followed by a sharp drop in TEC values occurring on August 11, 2025, and then by an increase from August 11 to August 20, 2025. A sharp decrease in TEC values was recorded on August 21, 2025, followed by an increase from August 22 to August 28, 2025.

From August 28 to September 3, 2025, TEC values greater than $\mu + 2\sigma$ were recorded (during these days, high solar activity and geomagnetic disturbances were observed; Figure 2 and Figure 5a). Then, from September 4 to September 9, 2025, a decrease in TEC values occurred. Such anomalies in the behavior of total electron content in the ionosphere preceded a series of earthquakes, including those with $M = 7.4$ and $M = 7.8$ that occurred on September 13 and September 19, 2025 (Figure 5a).

The analysis of time series of TEC characteristics obtained for 14 LT, presented in Figure 5b, demonstrated similar patterns in the anomalous TEC behavior during the preparation and occurrence of strong earthquakes. For this time of day, a notable feature was identified: a prolonged gradual decrease in TEC values. However, this period was longer than that identified using nighttime data for 2 LT. As indicated by the analysis of Figure 5b, the decrease in TEC values began on April 3, 2025, and continued for almost 3.5 months (until July 14, 2025). This decline in TEC values ended respectively 6 and 14 days before the onset of a series of strong earthquakes, including those with $M = 7.4$ and $M = 8.8$ (Figure 5b).

A similar pattern associated with a prolonged decrease in TEC (lasting more than a month) was also recorded before strong earthquakes with $M = 6.0$–7.8 that occurred in Türkiye in February 2023 [*Bondur et al.*, 2023].

Figure 6 presents a generalized diagram illustrating the registration of TEC $> \mu + 2\sigma$ and TEC $< \mu$ for each two-hour interval from January 1 to the end of September 2025.

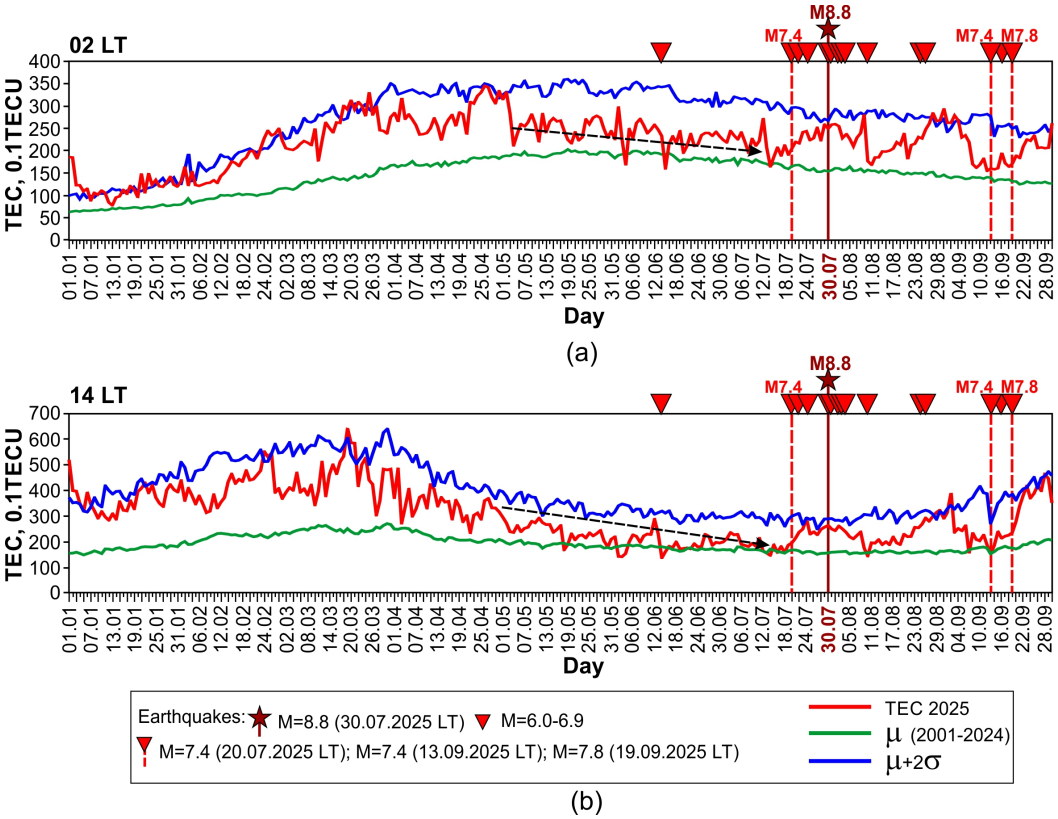

Figure 5. Time series of TEC (red solid line) from January 1 to September 30, 2025, long-term average TEC values from 2001 to 2024 (green line), $\mu + 2\sigma$ (blue line) for 2 LT (a) and 14 LT (b).

From the analysis of Figure 6 it follows that there are two main periods when TEC values exceed $\mu + 2\sigma$ for all two-hour intervals (except 6 LT):

- from January 1 to March 26, 2025.
- from August 28 to September 3, 2025.

In addition, high values of TEC > $\mu + 2\sigma$ were also recorded: from September 23 to September 29, 2025, at 14–18 LT; on September 28 and September 29, 2025 at 20 LT and 22 LT; on September 30, 2025 at 0 LT and 2 LT (Figure 6). TEC values below the long-term average were recorded mainly in the period from May 3 to July 19, 2025. Besides, for different hourly intervals, such TEC values appeared from August 9 to August 16, 2025 and from September 7 to September 18, 2025 (Figure 6).

From the analysis of Figure 6, it follows that during the studied period from January 1 to September 30, 2025, values of TEC below long-term average values typically were observed before earthquakes or on the days of earthquakes only if geomagnetic disturbances were recorded on the day of the earthquake or in the days immediately preceding and following it (Fig 2a).

3.4. Analysis of Relative Values of Total Electron Content in the Ionosphere

To identify ionospheric anomalies during the preparation and occurrence of earthquakes in the Kamchatka Peninsula region, changes in relative values of total electron content in the ionosphere (DTEC), recorded using GNSS data, were also analyzed for the period from January 1 to September 30, 2025. DTEC was calculated using a sliding window method as described above.

The two-dimensional distribution of DTEC is presented in Figure 7. Analysis of this Fig. shows that extensive negative DTEC anomalies were generally recorded on days of geomagnetic disturbances (Figure 2a). Extensive positive DTEC anomalies identified in

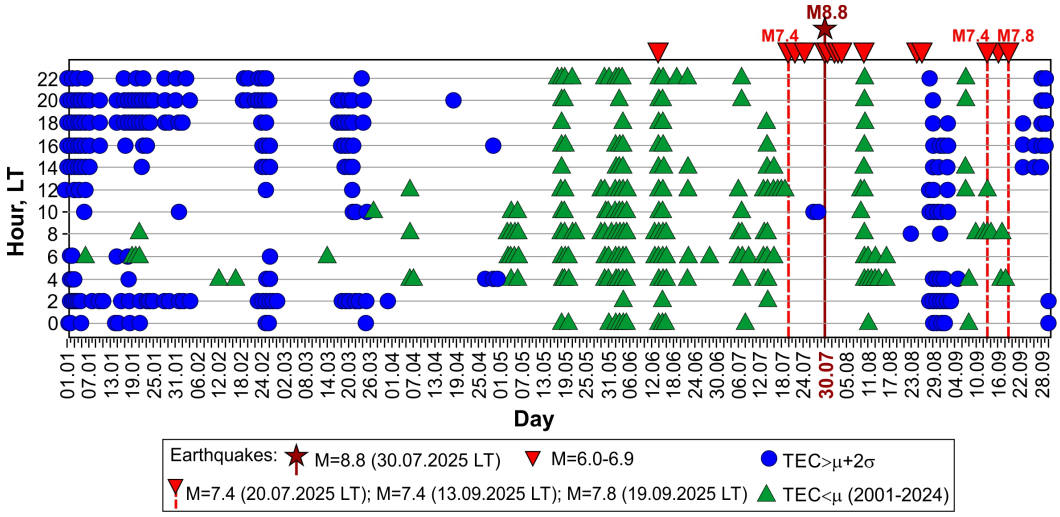

Figure 6. Generalized diagram of TEC > μ + 2σ, TEC < μ for each two-hour interval from January 1 to the end of September 2025.

January–February 2025, as well as from March 16 to March 20, 2025 and from August 23 to August 31, 2025, were registered on days of increased solar activity (Figure 7 and 2b).

Analysis of Figure 7 shows that from June 6 to June 10, 2025 (4–10 days before the *M*6.0 earthquake that occurred on June 14, 2025), a positive DTEC anomaly was registered from 0 LT to 12 LT and from 18 LT to 22 LT (Figure 7). A positive anomaly was also detected from 4 LT to 14 LT on July 22, 2025 and daylong from July 23 to July 25, 2025. It may be associated with both the process of earthquake preparation, including a powerful *M*8.8 earthquake on July 30, 2025, as well as its numerous strong aftershocks and with *M*6.0 foreshocks that were registered on July 22 and July 25, 2025.

The negative DTEC anomaly was recorded daylong (with minimum values detected at 8 LT and 12 LT) from July 12 to July 14, 2025 (i.e., 7–9 days before the *M*7.4 earthquake that occurred on July 20, 2025) (Figure 7).

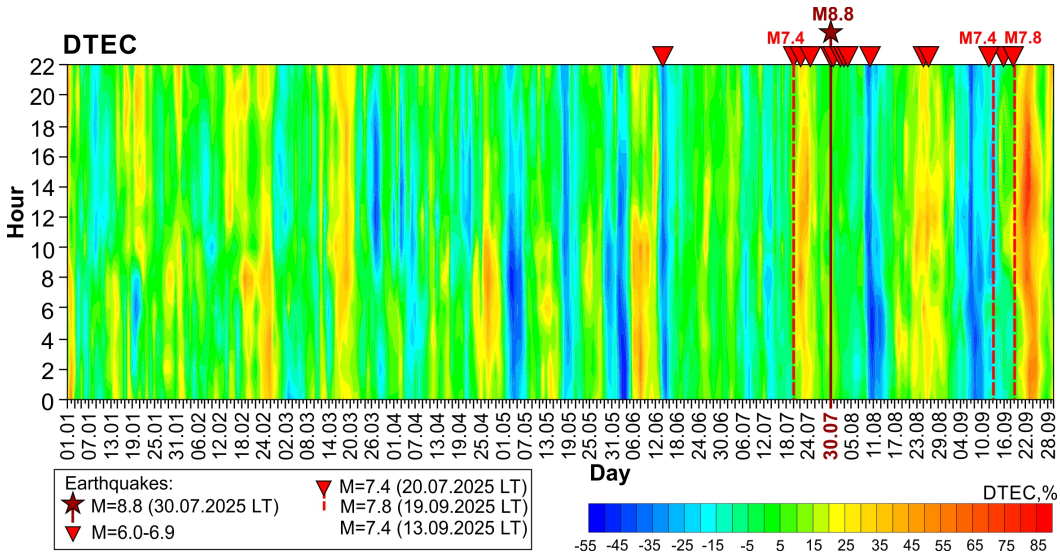

Figure 7. Two-dimensional DTEC distribution calculated using a sliding window method based on data from January 1 to September 28, 2025.

Global and regional DTEC maps for each two-hour interval were analyzed to confirm the connection between the anomalous changes in the ionosphere recorded from July 23 to July 25, 2025, and the preparation of the *M*8.8 earthquake that occurred on July 30, 2025, as well as its aftershocks with *M* = 6.0–6.9.

In Figure 8a, a global DTEC map for July 23, 2025 (4 LT) is presented as an example. The map clearly shows an extensive positive anomaly in the epicentral zone of the impending earthquake in the Kamchatka Peninsula area. The anomaly is located along a parallel. Its maximum size reaches up to 1000 km along the meridian and exceeds 6000 km along the parallel.

In Fig.s 8c, 9a, and 9b, regional DTEC maps are presented showing identified nighttime positive anomalies recorded at 4 LT on July 23, 2025 (DTEC = 36% in the epicentral area), as well as at 2 LT on July 24 and July 25, 2025 (DTEC = 22% and DTEC = 28%, respectively).

From the analysis of the DTEC time series for the morning hours (4 LT) from January 1 to September 30, 2025, presented in Figure 8b, it follows that on June 3, 2025 (11 days before the $M6.0$ earthquake on June 14, 2025), a drop in DTEC values was recorded, followed by an increase on June 8, 2025.

An analysis of Figure 8b demonstrated that a decrease in DTEC values was recorded from June 26 to July 7, 2025, followed by an increase (July 11, 2025), a decrease in DTEC values (July 13, 2025), and an overall increase that continued until July 23, 2025. At the same time, a slight decrease in DTEC values was detected on July 17, 2025 (3 days before the $M7.4$ earthquake that occurred on July 20, 2025) (Figure 8b).

A 37% decrease in DTEC values was detected on July 28, 2025 (2 days before the $M8.8$ earthquake that occurred on July 30, 2025) (Figure 8b). Additionally, the following were identified: a 13% decrease in DTEC values recorded on August 7, 2025 (3 days before the $M6.0$ earthquake that occurred on August 10, 2025); a 46% decrease in DTEC values recorded on September 8, 2025 (5 days before the $M7.4$ earthquake that occurred on September 13, 2025); and a 14% decrease in DTEC values recorded on September 18, 2025 (1 day before the $M7.8$ earthquake that occurred on September 19, 2025).

When analyzing the time series of DTEC values obtained for 2 LT (Figure 9c), patterns similar to those identified for such data recorded at 4 LT (Figure 8b) are observed.

3.5. Analysis of Normalized Values of Total Electron Content Using Neural Networks

Figure 10 shows NTEC time series obtained from long-term data using neural networks (LSTM and AE) for daytime (a) and nighttime (b) values, as well as $\mu+\sigma$, $\mu+2\sigma$, $\mu+3\sigma$ thresholds. A joint analysis of Figure 10a and 10b demonstrated their similarity, and any differences are minor. The methodology for using these neural networks is described above.

The analysis of Figure 10 identified time periods with NTEC values greater than $\mu+2\sigma$ and $\mu+3\sigma$. These anomalous outliers are most likely associated with geomagnetic disturbances and increased solar activity:

- On January 2, 2025, a strong geomagnetic disturbance was observed (Dst = −221 nT, Figure 2a), while moderate geomagnetic disturbances were recorded on January 4 and March 23, 2025 (Dst = −98 nT and Dst = −61 nT respectively, Figure 2a);
- High solar activity F10.7>200 sfu was registered on January 1–5, January 17–25, February 1–6, February 23–25, August 27–31, and on September 1–3, 2025 (Figure 2b).

From the analysis of Fig.s 10 a,b, it follows that from May 2 (based on daytime data) and from May 3 (based on nighttime data) to July 19, 2025, there was a decrease in NTEC values. It is important to note that during this period, small increases in NTEC values were recorded:

- Based on daytime and nighttime data, on June 2–4, 2025 (when strong geomagnetic disturbances were observed, Figures 2a and 10), and also on June 14, 2025, when an $M6.0$ earthquake occurred along with strong geomagnetic disturbances (Figures 2a and 10);
- Based on daytime data, an increase in NTEC values was also identified on June 12, 2025 (two days before an $M6.0$ earthquake).

For the period from June 16 to July 19, 2025, both daytime and nighttime data showed very low NTEC values without significant spikes (Figure 10a, b).

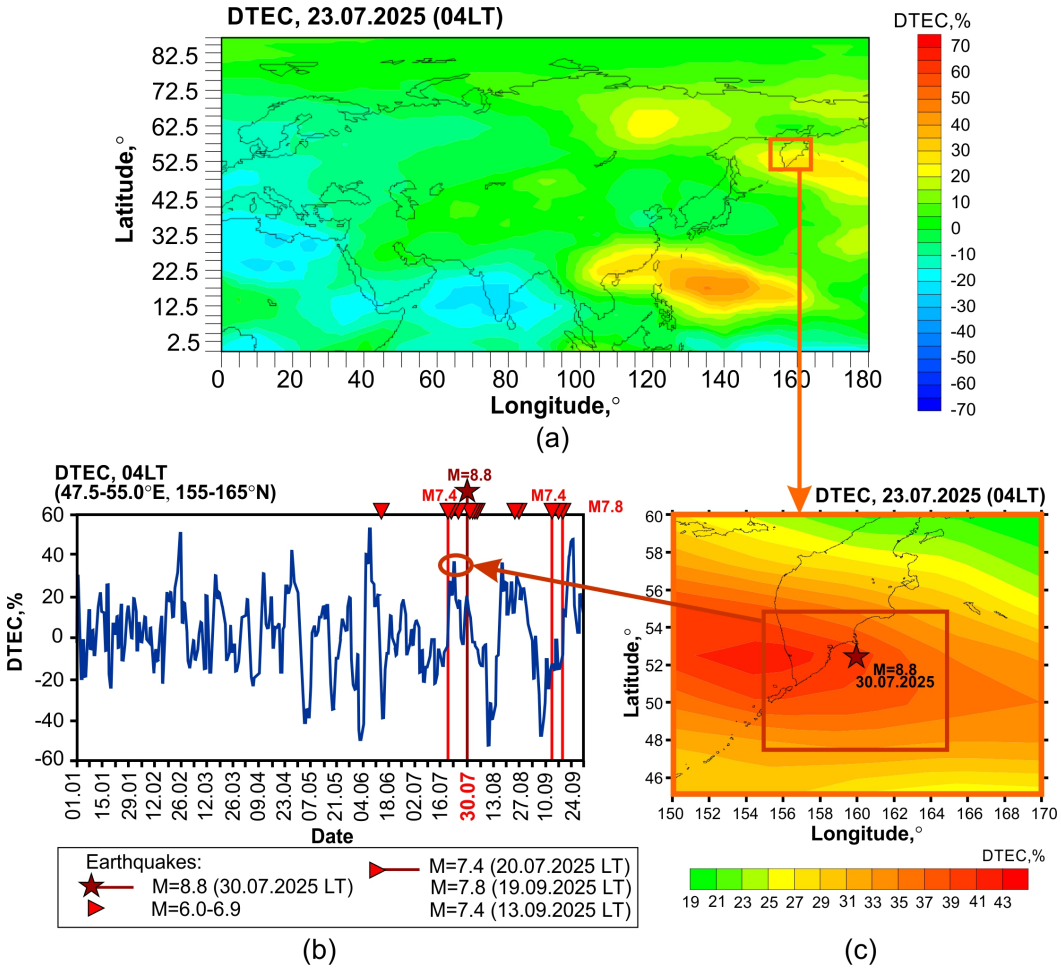

Figure 8. Global DTEC map (a) and regional DTEC map (c) with identified anomalies on July 23, 2025 (4 LT), and the time series of DTEC from January 1 to September 30, 2025, for 4 LT (b).

Starting from July 21, 2025, both daytime and nighttime data revealed an increase in NTEC values. A decrease in these values was observed on July 25 and July 26, 2025 (4 and 5 days before the M8.8 earthquake, which occurred on July 30, 2025).

The pattern of NTEC changes recorded from July 27 to August 17, 2025, based on daytime and nighttime data, differed slightly. For nighttime data, an increase in NTEC values was recorded from July 27 to July 31, 2025; then, a decrease occurred from August 1 to August 5, 2025, followed by an increase in NTEC values until August 8, 2025, and then a decrease that continued until August 17, 2025 (Figure 10b).

For daytime data, an increase in NTEC values was recorded on July 27 and July 28, 2025, while on July 29, 2025 (one day before the M8.8 earthquake on July 30, 2025), a decrease in NTEC values was registered. NTEC values remained low on the day of the earthquake on July 30, 2025 (Figure 10a). On July 31, 2025, an increase in these values was registered, followed by an overall downward trend in NTEC values from August 3 to August 17, 2025.

From August 22, 2025, both nighttime and daytime data showed an increase in NTEC values, which peaked on August 29, 2025, exceeding the long-term average values (μ) (Figure 10). NTEC values greater than μ were also recorded on August 31 and September 1, 2025 (based on nighttime data) and on September 21 and September 2, 2025 (based on daytime data). During these days, geomagnetic disturbances and high solar activity were recorded (Figures 2 and 10). Starting from September 3, 2025, a decrease in NTEC values was registered, lasting until September 7, 2025. Low NTEC values were observed until September 19, 2025 (before and during earthquakes occurred on September 13, 2025, with M = 7.4 and September 19, 2025, with M = 7.8).

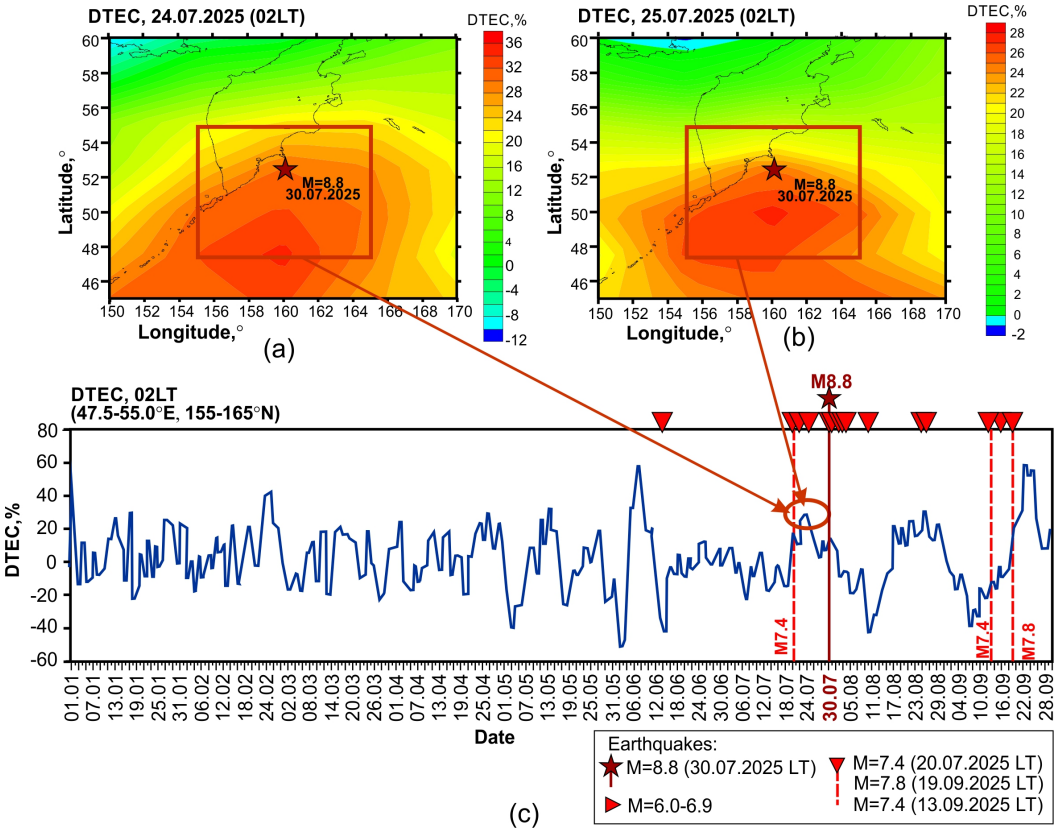

Figure 9. Regional DTEC maps with identified anomalies recorded on July 24, 2025 (a) and July 25, 2025 (b) at 2 LT, and DTEC time series from January 1 to September 30, 2025, for 02 LT (c).

Thus, the analysis of NTEC time series using neural networks (LSTM and AE) revealed changes similar to those identified in the TEC analysis (Figure 5, Figure 6), DTEC (Figures 7–9), while also excluding the outliers of these TEC characteristics related to geomagnetic disturbances and solar activity from the analysis.

Table 2 presents identified changes in ionospheric parameters that may be associated with the preparation and occurrence of strong earthquakes with $M \geq 6$ from June to September 2025. It should be noted that strong geomagnetic disturbances (Dst = −101 to −221 nT) were recorded on January 2, April 17, June 1–3, and June 14, 2025 (Figure 2a); moderate geomagnetic disturbances (Dst = −50– −98 nT) were identified on January 4, 9, 13, 23, and March 27, as well as on August 9, 3, 15 and September 30, 2025 (Figure 2a).

Additionally, high solar activity (F10.7 > 200 sfu) was also registered on January 1–5, January 17–25, February 1–6, February 23–25, August 27–31 and September 1–3, 2025 (Figure 2b).

Changes in ionospheric parameters that were recorded during periods of geomagnetic disturbances and high solar activity and might be associated with these disturbances were not included in Table 2.

From June 16 to August 8, 2025, no geomagnetic disturbances were recorded, and solar activity was relatively weak. Therefore, the observed anomalous changes in ionospheric parameters may be associated with the preparation of the earthquakes that occurred in July–August 2025.

From the data presented in Table 2, it follows that the analysis of N_e, TEC, DTEC, and NTEC revealed the anomalies in the ionosphere that may be related to the preparation and occurrence of strong earthquakes with $M \geq 6$ from June to September 2025, including the $M8.8$ earthquake (July 30, 2025). These anomalies were primarily manifested as follows:

- a decrease in the ionospheric electron density N_e (by 8–23%) detected 1–6 days before earthquakes with magnitudes M = 6.0–8.8 that occurred near the Kamchatka Penin-

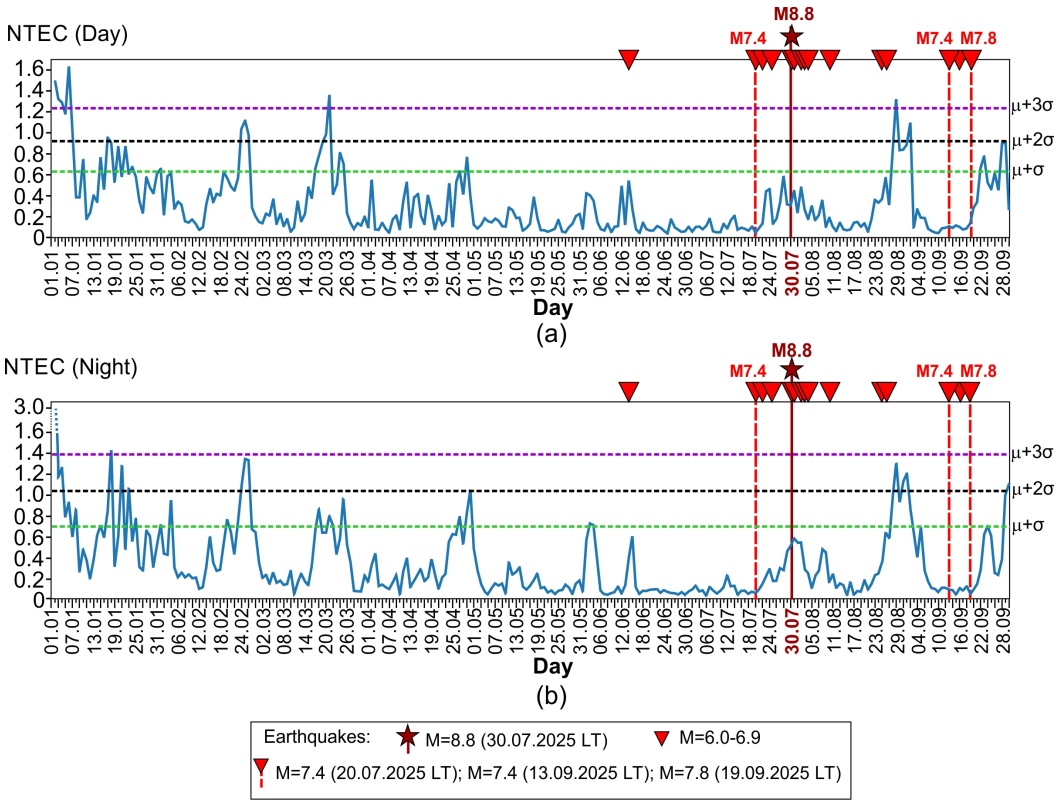

Figure 10. Analysis of NTEC time series calculated from multi-year data (2001–2025) using neural networks (LSTM and AE): a – daytime values; b – nighttime values.

sula in June–September 2025 and an increase in N_e (by 7–20%) detected 3, 5, and 8 days before them;

- a general decrease in TEC values (~15–50%) from May 3 to July 14, 2025, and an increase in TEC values (~30%) from July 15 to July 24, 2025, before and during strong earthquakes with $M \geq 6.0$, including a powerful $M8.8$ earthquake, in June–July 2025;
- a local positive nighttime anomaly that appeared at 2 LT and 4 LT with DTEC = 22–36%, its spatial dimensions were about 1000 km along the meridian and more than 6000 km along the parallel.

It should be pointed out that in other works, for example, [*Bondur and Smirnov*, 2005; *Bondur et al.*, 2024, 2022, 2021; *Liperovsky et al.*, 1992; *Pulinets and Boyarchuk*, 2004; *Smirnov et al.*, 2018; *Zolotov et al.*, 2013], the main features of ionospheric anomalies during the preparation and occurrence of earthquakes were identified; they can be summarized as follows:

- ionospheric anomalies are variations in ionospheric plasma (deviations from the undisturbed value), observed in the near-epicentral area, as a rule, 1–5 days before strong earthquakes ($M \geq 6.0$), but can appear earlier (the sign of the variations can be both positive and negative);
- seismo-ionospheric variations can have the same amplitude as the diurnal variability of the ionosphere (10%–15%), but can also reach higher values (>30–90%);
- the maximum of the anomalous area in the ionosphere may not coincide with the vertical projection of the epicenter of the future earthquake;
- the sizes of the anomaly zones are approximately 1000 km along the meridian and several thousand kilometers along the parallel;
- the development of the ionospheric anomaly can be accompanied by a change in sign.

Moreover, in the work [*Pulinets et al.*, 2021], it was shown that positive TEC deviations are most often observed in the time interval from 18 LT to 6 LT the following day.

Table 2. Changes in ionospheric parameters during the preparation and occurrence of strong earthquakes with $M \geq 6$ from June to September 2025

Parameter	Identified anomalies
N_e	A decrease (by 8–23%) 2, 4, and 6 days before the $M7.4$ earthquake (July 20, 2025); and an increase (by 7–17%) 3 and 5 days before it. An increase (by 12–20%) 8 days before a massive $M8.8$ earthquake (July 30, 2025), and a decrease (by 9–18%) 1, 2, and 5 days before it.
TEC	**Nighttime data.** • Decrease in values: – May 3– July 14, 2025 (~15–50%) – July 14, 2025 (TECμ), 6 days before the $M7.4$ earthquake (July 20, 2025) – July 25–26, 2025 (by ~10%), July 28, 2025 (by ~12%), 4–5 days and 2 days before the $M8.8$ earthquake (July 30, 2025) – August 21, 2025 (by ~36%), 4 days before the $M6.1$ earthquake (August 25, 2025) – 4–September 9, 2025 (by ~43%), 4–9 days before the $M7.4$ earthquakes (September 13, 2025) and 10–15 days before the $M7.8$ earthquake (September 19, 2025) • Increase in values: – July 15–24, 2025 (by ~35%), 6–15 days before the earthquakes with $M \geq 6$ recorded from July 20, 2025 to July 31, 2025 – August 11–20, 2025 (by ~31%), 5–16 days before the earthquakes with $M = 6.1$ (August 25, 2025) and $M = 6.0$ (August 27, 2025) **Daytime data.** • Decrease in values: – April 3, 2025 – July 14, 2025 (by ~60%) – September 7, 2025 (by ~44%), 6 days before the $M7.4$ earthquake (September 13, 2025) – September 16, 2025 (by ~16%), 3 days before the $M7.8$ earthquake (September 19, 2025) • Increase in values: – July 18–24, 2025 (by ~50%), 2 days before the earthquakes with $M = 6.6$–7.4 (July 20, 2025), 4 days before the $M6.0$ earthquake (July 22, 2025) and during these earthquakes, 1–7 days before the $M6.0$ earthquake (July 25, 2025), 6–12 days before the $M8.8$ earthquake (July 30, 2025)
DTEC (two-dimensional distribution)	Positive anomaly: • June 6–10, 2025, from 0 LT to 12 LT and from 18 LT to 22 LT (4–10 days before the $M6.0$ earthquake (June 14, 2025)) • July 22, 2025 (from 4 LT to 14 LT), July 23–25, 2025, 5–8 days before a powerful $M8.8$ earthquake (July 30, 2025)
DTEC (global and regional maps)	Nighttime positive anomaly (DTEC = 22–36%) in the epicentral area: July 23–25, 2025 (2 LT and 4 LT) reaches 1000 km along the meridian, and exceeds 6000 km along the parallel, 5–7 days before a powerful $M8.8$ earthquake (July 30, 2025).
NTEC	**Nighttime data.** • Decrease in values: – May 3 – July 19, 2025 – July 25, 2025 and July 26, 2025, 4 and 5 days before a powerful $M8.8$ earthquake (July 30, 2025) – August 1–5, 2025 – August 10–17, 2025 • Increase in values: – July 21–24, 2025 – July 27–31, 2025 **Daytime data.** • Decrease in values: – May 2 – July 19, 2025 – July 25, 2025 and July 26, 2025 (4 and 5 days before a powerful $M8.8$ earthquake (July 30, 2025)) – July 29, 2025, 1 day before a powerful $M8.8$ earthquake (July 30, 2025) – August 3–17, 2025 • Increase in values: – June 12, 2025 – July 21–24, 2025 – July 27–28, 2025

Thus, the aforementioned anomalous changes in the ionosphere recorded by satellite navigation system data during the preparation and occurrence of a powerful $M8.8$ earthquake on July 30, 2025, as well as other strong earthquakes with $M \geq 6$ that occurred

from June to September 2025 near the Kamchatka Peninsula, correspond to the main characteristics of ionospheric anomalies that arise during the preparation and occurrence of earthquakes described in works [*Bondur and Smirnov*, 2005; *Bondur et al.*, 2024, 2022, 2021; *Liperovsky et al.*, 1992; *Pulinets and Boyarchuk*, 2004; *Smirnov et al.*, 2018; *Zolotov et al.*, 2013].

4. Conclusion

The paper presents the results of research on satellite navigation system data regarding changes occurred in the ionosphere during the preparation and occurrence of earthquakes with $M \geq 6$ in the Kamchatka Peninsula region from June to September 2025, including a powerful tsunamigenic $M8.8$ earthquake that occurred on July 29, 2025, UTC (July 30, 2025, LT). The study analyzed altitude changes in ionospheric electron density (N_e), total electron content of the ionosphere (TEC), relative changes in total electron content of the ionosphere (DTEC), and normalized values of total electron content of the ionosphere (NTEC) using various methodologies, including artificial neural networks.

The analysis of N_e altitude profiles revealed quasi-periodic variations, which were clearly observed as a decrease in N_e values by 8–23% occurring 2, 4, and 6 days prior, as well as an increase in N_e values by 7–17%, recorded 3 and 5 days before the $M7.4$ earthquake occurred on July 20, 2025. Additionally, an increase in N_e values by 12–20% was identified 8 days prior and a decrease in N_e values by 9–18% was observed 1, 2, and 5 days before a powerful $M8.8$ earthquake that occurred on July 30, 2025, LT (July 29, 2025, UTC).

Based on the results of the study of TEC variations from nighttime data, it was found that there was a general decrease in TEC values from May 3 to July 14, 2025. Daytime data also registered a decrease in TEC values; however, this period was longer, lasting for 3.5 months (from April 3 to July 14, 2025). TEC values lower than the long-term average were observed 10 days before the $M6.0$ earthquake that occurred on June 14, 2025, and 6 days before the $M7.4$ earthquake that occurred on July 20, 2025.

It was found that from July 21, 2025, there was an increase in TEC values that continued until July 24, 2025, followed by a decrease in these values 4–5 days prior and then again 2 days before a massive tsunamigenic $M8.8$ earthquake and its foreshocks with M = 6.0–6.9 that occurred on July 30, 2025, LT (July 29, 2025, UTC). A decrease in TEC values was also identified 4 days before the $M6.1$ earthquake that occurred on August 5, 2025, as well as from September 4 to September 9, 2025, before the earthquakes with M = 7.4 (September 13, 2025) and M = 7.8 (September 19, 2025).

The analysis of relative values of total electron content of the ionosphere revealed a nighttime positive anomaly (DTEC=22–36%) in the epicentral area at 2 LT and 4 LT, which manifested 5–7 days before a powerful $M8.8$ earthquake. This anomaly extended along a parallel for more than 6000 km, while its meridional extent reached up to 1000 km.

The analysis of time series of normalized values of total electron content (NTEC), calculated from long-term data (from 2001to 2025) using artificial neural networks (Long Short-Term Memory (LSTM) and Autoencoder (AE)), allowed for the identification of abnormal changes in NTEC that are likely related to periods of geomagnetic disturbances and high solar activity. Through neural network analysis of NTEC, a period of very low NTEC values without significant spikes was also identified (from June 16 to July 19, 2025). This period preceded a series of strong earthquakes ($M \geq 6$) that began on July 20, 2025. From July 21, 2025, an increase in NTEC values was observed along with a decrease occurring 4 and 5 days before the $M8.8$ earthquake, followed by another increase in NTEC until July 31, 2025. From August 3 to August 17, 2025, a general downward trend in NTEC values was registered. Low NTEC values were also recorded from September 7 to September 19, 2025, before and during the earthquakes with M = 7.4 (September 13, 2025) and M = 7.8 (September 19, 2025).

Thus, the analysis of N_e altitude profiles, as well as time series of TEC, DTEC, and NTEC, allowed for the identification of similar patterns in the changes of these parameters

during the preparation and occurrence of strong earthquakes with $M \geq 6$ from June to September 2025, including a powerful $M8.8$ earthquake that occurred on July 30, 2025. The identified patterns correspond to the main characteristics of ionospheric anomalies that arise during preparation and occurrence of strong earthquakes, as described in earlier studies.

The analysis of ionospheric variations and heliogeophysical conditions revealed anomalous changes in the ionosphere that may also be related to geomagnetic disturbances and solar activity, and allowed for their exclusion from the analysis. It is important to note that from June 16 to August 8, 2025, no geomagnetic disturbances were recorded, and solar activity was low. Therefore, the identified abnormal changes in ionospheric parameters during this period might be associated with the processes of preparation and occurrence of earthquakes in the Kamchatka Peninsula region in July–August 2025.

Acknowledgments. The research was carried out in the framework of the state assignment of ISR "AEROCOSMOS".

References

Akhoondzadeh M., De Santis A., Marchetti D., et al. Multi precursors analysis associated with the powerful Ecuador (MW = 7.8) earthquake of 16 April 2016 using Swarm satellites data in conjunction with other multi-platform satellite and ground data // Advances in Space Research. — 2018. — Vol. 61, no. 1. — P. 248–263. — https://doi.org/10.1016/j.asr.2017.07.014

Bhandarkar T., Vardaan K., Satish N., et al. Earthquake trend prediction using long short-term memory RNN // International Journal of Electrical and Computer Engineering (IJECE). — 2019. — Vol. 9, no. 2. — P. 1304–1312. — https://doi.org/10.11591/ijece.v9i2.pp1304-1312

Bondur V. G. and Smirnov V. M. Method for monitoring seismically hazardous territories by ionospheric variations recorded by satellite navigation systems // Doklady Earth Sciences. — 2005. — Vol. 403, no. 5. — P. 736–740.

Bondur V. G., Tsidilina M. N., Gaponova E. V., et al. Satellite Registration of Anomalies of Various Geophysical Fields during the Preparation of Destructive Earthquakes in Turkey in February 2023 // Izvestiya, Atmospheric and Oceanic Physics. — 2023. — Vol. 59, no. 9. — P. 1009–1027. — https://doi.org/10.1134/s0001433823090049

Bondur V. G., Tsidilina M. N., Gaponova E. V., et al. Satellite-Detected Anomalous Changes in Parameters of Various Geophysical Fields During Earthquakes of $6 \leq M \leq 7.8$ in Türkiye in February 2023 // Russian Journal of Earth Sciences. — 2024. — Vol. 24. — ES4006. — https://doi.org/10.2205/2024es000930

Bondur V. G., Tsidilina M. N., Gaponova E. V., et al. Combined Analysis of Anomalous Variations in Various Geophysical Fields during Preparation of the M5.6 Earthquake near Lake Baikal on September 22, 2020, Based on Satellite Data // Izvestiya, Atmospheric and Oceanic Physics. — 2022. — Vol. 58, no. 12. — P. 1532–1545. — https://doi.org/10.1134/s0001433822120052

Bondur V. G., Tsidilina M. N., Voronova O. S., et al. A Study from Space of Anomalous Variations of Various Geophysical Fields during the Preparation of a Series of Strong Earthquakes in Italy in 2016-2017 // Izvestiya, Atmospheric and Oceanic Physics. — 2021. — Vol. 57, no. 12. — P. 1604–1620. — https://doi.org/10.1134/s0001433821120057

Bychkov V. V., Smirnov S. E., Korsunova L. P., et al. Atmospheric anomalies and anomalies of electricity in the near-surface atmosphere before the Kamchatka earthquake of January 30, 2016, based on the data from the Paratunka Observatory // Geomagnetism and Aeronomy. — 2017. — Vol. 57, no. 4. — P. 491–499. — https://doi.org/10.1134/s0016793217040053

Chebrov V. N., Saltykov V. A. and Serafimova Y. K. Identifying the precursors of large ($M \geq 6.0$) earthquakes in Kamchatka based on data from the Kamchatka Branch of the Russian expert council on earthquake prediction: 1998-2011 // Journal of Volcanology and Seismology. — 2013. — Vol. 7, no. 1. — P. 76–85. — https://doi.org/10.1134/s074204631301003x

Dobrovolsky I. P., Zubkov S. I. and Myachkin V. I. Estimation of the size of earthquake preparation zones // Pure and Applied Geophysics. — 1979. — Vol. 117, no. 5. — P. 1025–1044. — https://doi.org/10.1007/bf00876083

Fedotov S. A. Long-Term Earthquake Prediction for the Kuril-Kamchatka Arc. — Moscow : Nauka, 2005. — 302 p. — (In Russian).

Freund F. Pre-earthquake signals: Underlying physical processes // Journal of Asian Earth Sciences. — 2011. — Vol. 41, no. 4/5. — P. 383–400. — https://doi.org/10.1016/j.jseaes.2010.03.009

Gokhberg M. B. and Shalimov S. L. Lithosphere-ionosphere relation and its modeling // Russian Journal of Earth Sciences. — 2000. — Vol. 2, no. 2. — P. 95–108. — https://doi.org/10.2205/2000es000032 — (In Russian).

Liperovsky V. A., Pokhotelov O. A., Liperovskaya E. V., et al. Physical models of coupling in the lithosphere-atmosphere-ionosphere system before earthquakes // Geomagnetism and Aeronomy. — 2008. — Vol. 48, no. 6. — P. 795–806. — https://doi.org/10.1134/s0016793208060133

Liperovsky V. A., Pokhotelov O. A. and Shalimov S. L. Ionospheric earthquake precursors. — Moscow : Nauka, 1992. — 304 p. — (In Russian).

Mogi K. Earthquake Prediction. — Tokyo : Academic Press, 1985. — 355 p.

Namgaladze A. A. and Karpov M. I. Conduction current and extraneous electric current in the global electric circuit // Russian Journal of Physical Chemistry B. — 2015. — Vol. 9, no. 5. — P. 754–757. — https://doi.org/10.1134/s1990793115050231

Natural Hazards of Russia. Vol. 2. Seismic Hazards / ed. by G. A. Sobolev. — Moscow : KRUK, 2000. — 296 p. — (In Russian).

Noll C. The crustal dynamics data information system: A resource to support scientific analysis using space geodesy // Advances in Space Research. — 2010. — Vol. 45, no. 12. — P. 1421–1440. — https://doi.org/10.1016/j.asr.2010.01.018

Oskorbin L. S., Poplavsky A. A., Streltsov M. I., et al. Neftegorsk earthquake of 27 May 1995 (Mw = 7.1) // Earthquakes in Northern Eurasia in 1995. — Moscow : GS RAS, 2001. — P. 170–182. — (In Russian).

Parrot M., Tramutoli V., Liu T. J. Y., et al. Atmospheric and ionospheric coupling phenomena related to large earthquakes // Natural Hazards and Earth System Sciences. — 2016. — https://doi.org/10.5194/nhess-2016-172

Pulinets S., Tsidilina M., Ouzounov D., et al. From Hector Mine M7.1 to Ridgecrest M7.1 Earthquake. A Look from a 20-Year Perspective // Atmosphere. — 2021. — Vol. 12, no. 2. — P. 262. — https://doi.org/10.3390/atmos12020262

Pulinets S. A., Bondur V. G., Tsidilina M. N., et al. Verification of the concept of seismoionospheric coupling under quiet heliogeomagnetic conditions, using the Wenchuan (China) earthquake of May 12, 2008, as an example // Geomagnetism and Aeronomy. — 2010. — Vol. 50, no. 2. — P. 231–242. — https://doi.org/10.1134/s0016793210020118

Pulinets S. A. and Boyarchuk K. Ionospheric Precursors of Earthquakes. — Berlin : Springer-Verlag, 2004. — 315 p. — https://doi.org/10.1007/b137616

Pulinets S. A., Ouzounov D. P., Karelin A. V., et al. Physical bases of the generation of short-term earthquake precursors: A complex model of ionization-induced geophysical processes in the lithosphere-atmosphere-ionosphere-magnetosphere system // Geomagnetism and Aeronomy. — 2015. — Vol. 55, no. 4. — P. 521–538. — https://doi.org/10.1134/s0016793215040131

Smirnov V. M., Smirnova E. V., Tsidilina M. N., et al. Seismo-Ionospheric Variations during Strong Earthquakes Based on the Example of the 2010 Earthquake in Chile // Cosmic Research. — 2018. — Vol. 56, no. 4. — P. 267–275. — https://doi.org/10.1134/s0010952518040068

Sobolev G. A. and Ponomarev A. V. Earthquake physics and precursors. — Moscow : Nauka, 2003. — 270 p. — (In Russian).

Sorokin V. M. and Hayakawa M. Generation of seismic-related DC electric fields and lithosphere-atmosphere-ionosphere coupling // Modern Applied Science. — 2013. — Vol. 7, no. 6. — P. 1–25. — https://doi.org/10.5539/mas.v7n6p1

Sorokin V. M. and Ruzhin Y. Y. Electrodynamic model of atmospheric and ionospheric processes on the eve of an earthquake // Geomagnetism and Aeronomy. — 2015. — Vol. 55, no. 5. — P. 626–642. — https://doi.org/10.1134/s0016793215050163

Xue J., Huang Q., Wu S., et al. LSTM-Autoencoder Network for the Detection of Seismic Electric Signals // IEEE Transactions on Geoscience and Remote Sensing. — 2022. — Vol. 60. — P. 1–12. — https://doi.org/10.1109/tgrs.2022.3183389

Yurtin A. A. Towards a loss function for training neural network models of time series imputation // Bulletin of the South Ural State University. Series "Computational Mathematics and Software Engineering". — 2024. — Vol. 13, no. 4. — P. 53–73. — https://doi.org/10.14529/cmse240404 — (In Russian).

Zhu F. and Jiang Y. Investigation of GIM-TEC disturbances before M ≥ 6.0 inland earthquakes during 2003-2017 // Scientific Reports. — 2020. — Vol. 10, no. 1. — https://doi.org/10.1038/s41598-020-74995-w

Zolotov O. V., Namgaladze A. A. and Prokhorov B. E. Specific features of ionospheric total electron content variations in the periods of preparation of the earthquakes on March 11, 2011 (Japan) and October 23, 2011 (Turkey) // Russian Journal of Physical Chemistry B. — 2013. — Vol. 7, no. 5. — P. 599–605. — https://doi.org/10.1134/s1990793113050266